Neumann et al. *EPJ Techniques and Instrumentation* (2021) 8:17
https://doi.org/10.1140/epjti/s40485-021-00074-7

EPJ Techniques and Instrumentation

RESEARCH ARTICLE Open Access

Thrust measurement and thrust balance development at DLR's electric propulsion test facility

Andreas Neumann[1*], Jens Simon[1] and Jens Schmidt[1]

*Correspondence:
a.neumann@dlr.de
[1]German Aerospace Center (DLR), Institute of Aerodynamics and Flow Technology, Bunsenstrasse 10, 37073, Goettingen, Germany

Abstract

Electric space propulsion thrusters only produce low thrust forces. For the fulfillment of a space mission this implies long thruster runtimes, and this entails long qualification times on ground. For such long testing times, a ground facility requires a vacuum chamber and a powerful pumping system which can guarantee high vacuum over extended times and under thruster gas load. DLR's STG-ET is such a ground test facility. It has a high pumping capability for the noble gases typically used as propellants. One basic diagnostic tool is a thrust measurement device, among various other diagnostic systems required for electric propulsion testing, e.g. beam diagnostics. At DLR we operate a thrust balance developed by the company AST with a thrust measurement range of 250 mN and capable of thruster weights up to 40 kg. Adversely, it is a bulky and heavy device and all upgrades and qualification work needs to be done in a large vacuum chamber. In order to have a smaller device at hand a second thrust stand is under development at DLR. The idea is to have a light and compact balance that could also be placed in one of the smaller DLR vacuum chambers. Furthermore, the calibration is more robust and the whole device is equipped with a watercooled housing. First tests are promising and showed a resolution well below 1 mN. In this paper we give background information about the chamber, describe the basics of thrust measurement and the development of a new balance.

Keywords: Electric space propulsion; Vacuum chamber; Test facility; Thrust balance

Introduction

Electric space propulsion is taking over more and more applications from chemical propulsion systems. Being common for attitude and station keeping, recent satellite missions also use electric thrusters for orbital maneuvers, e.g. from GTO to GEO [1]. The main advantages of electric propulsion are their very high propellant economy and a good controllability. On the other hand, the absolute thrust values of electric thrusters are low compared to their mass and power consumption, and this requires quite long firing times [2]. This entails the need for long on-ground testing, which has to be done under adequate vacuum conditions. Furthermore, the diagnostics equipment needed for qualification of

electric thrusters is quite different from chemical propulsion diagnostics. Thrust measurement is common for both techniques, but electric propulsion requires force measurement in a lower range and a long-term stability, due to the required long firing times. Therefore, the design and construction of an accurate thrust balance for electric propulsion is quite challenging. This is mainly driven by two constraints: very low thrust forces in the range of mN down to μN, depending on the type of thruster, need to be accurately measured whilst EP thrusters have a very low thrust-to-mass ratio, often below 1:1000. Thus, even a small error can reveal a very different system performance. Additionally, the long-term thermal drift of the thrust balance needs to be controlled, since most electric propulsion devices heat up due to thermal losses within their systems. Within a vacuum environment, thermal control is very challenging, since convection cannot be used as the major process of heat transfer and therefore the system has to be thermally stabilized either radiative or by heat conduction using cooling water or electrical heating. Water cooling, in turn, requires additional supply lines to the thruster which affect thrust measurements by temperature and position sensitive tension forces which can easily reach the measurement range of mN. Dealing with these constraints makes thrust measurement a crucial diagnostics task. This paper will focus on thrust balances as a basic equipment for investigating thrusters, and show details about thrust balances available at DLR.

The STG-ET facility of the German Aerospace Center (DLR) in Göttingen is one of the largest test facilities for electric propulsion worldwide [3], in which the use of thrust balances is essential for commercial and scientific users of the facility. The next sections show details of this facility and its diagnostic packages.

The STG-ET facility

This section describes the capabilities of DLR's STG-ET facility, which has been built specifically for simulation of a space environment and to test electric propulsion systems. For electric propulsion development and testing a variety of diagnostic methods are required and integrated in the STG-ET facility. Concerning measurement equipment, the focus within this work is on thrust measurement, one of the basic parameters to be controlled on thrusters. More details about the STG-ET facility and the available diagnostic measurement systems are given in [4].

The STG-ET facility is shown in Fig. 1 and consists of a large vacuum chamber with an inner diameter of 5 m and a length of 12.2 m. To create a rough vacuum, a large pump stand is used, containing a rotating vane pump and a Roots pump. Fine vacuum is created using 4 Edwards turbomolecular pumps connected to a second, smaller set of vane/Roots roughing pumps, reaching a stand-by pressure in the order of 10^{-6} mbar. The pumping speed can be significantly increased by the use of 18 Oerlikon Leybold cryopumps reaching a stand-by pressure in the low 10^{-7} mbar range [4]. Pumping speeds for gas flow rates for argon, krypton, and xenon released into the chamber at room temperature are 276,000 l/s for xenon, 360,000 l/s for krypton, and 452,000 l/s for argon.

Multiple diagnostic systems are available within the facility [4]. There are several moving arms to support the installation of diagnostics for plasma and ion beams. The C-Scanner, a C-shaped arm with 15 Faraday cups, is permanently installed to measure the beam current from electric propulsion devices as well as thrust stands for propulsion. The gas composition can be analyzed with a mass spectrometer. A large number of vacuum feedthroughs allows the simple installation of additional diagnostics to support experiments and the use

Figure 1 View of the STG-ET vacuum chamber with open door

of optical measurement methods through multiple windows. To shield the chamber walls from sputtering due to high energetic ions from propulsion, a water-cooled graphite target is installed at the rear end of the chamber and the chamber walls are partly protected with graphite sheets. As displayed in Fig. 1 the whole front-end lid of the chamber can be removed allowing easy access and installation of diagnostic equipment and thrusters. The vacuum chamber can operate continuously at low pressures for extended periods of time up to several weeks or months, giving a unique opportunity for long-duration testing of electric thrusters.

Thrust balance basics

Electric propulsion thrusters produce only a low thrust at high exit velocities due to the low mass flows required for operation to create the necessary plasma, resulting in their high fuel efficiency. Nevertheless, it is very important to measure these low forces with adequate precision in order to precisely determine the resulting change of momentum acting on the spacecraft. The instrument for this task is a thrust balance. There are various basic designs for such a task and in the literature general requirements and recommendations can be found [5, 6]. Figure 2 shows some of the most common design approaches used in EP facilities around the world [7]. In Fig. 2(a) one can see a simple vertical weigh cell used for thrust force measurement, but in this case the cell has to carry all the weight of the thruster assembly. Figure 2(b) is a single arm normal pendulum, a design that is used very often [8–10]. If very small forces have to be measured the torsional pendulum in (c) offers high sensitivity [11–15]. Figure 2(d) shows the inverted pendulum, which is not stable in the top position and requires active control that keeps it in the upper position. Adding a second crossmember gives the inverted double pendulum in sketch (e) [16–18]. This is a more robust design but still requires active control [19, 20]. Add a platform for counterbalancing leads to a design like (f), the counterbalanced inverted double pendulum. By

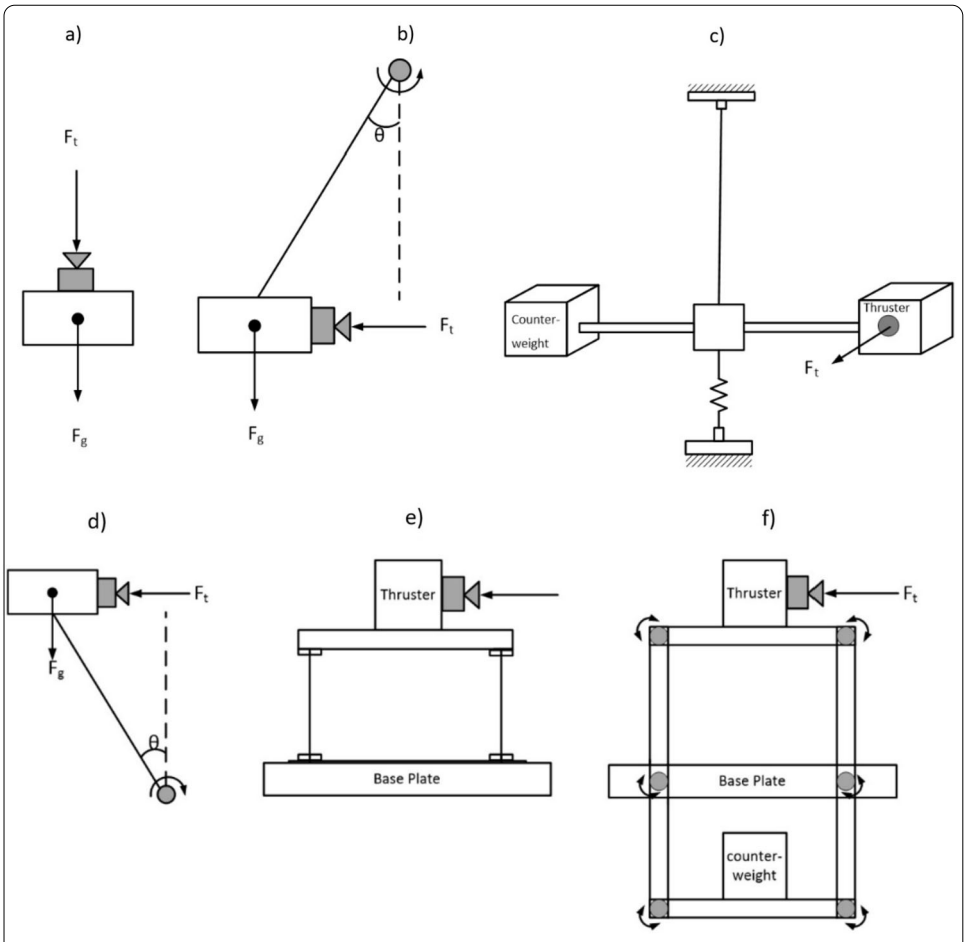

Figure 2 Some common design options for a thrust balance: (**a**) vertical weigh cell, (**b**) normal pendulum, (**c**) torsional pendulum, (**d**) inverted pendulum, (**e**) inverted double pendulum, (**f**) counterbalanced inverted double pendulum. Remark for (**b**) and (**d**): the thruster will be tilted too, but for simplification this is neglected in the picture, modified from [7]

trimming the weight, this system can be very sensitive. As a short remark for (b) and (d) one can add that the thruster and its force will be tilted too, but for simplification this is neglected in the picture. Table 1 summarizes the main advantages and disadvantages of the basic design concepts shown in Fig. 2.

All these designs have their pro's and con's as can be seen in Table 1, and a decision depends on the envisaged thruster mass, thrust range, accuracy, and the effort that has to go into design and construction. Thrust measurement may also be extended in two dimensions, which may be needed for engines with thrust vector control. Thrust balances for such an application were built, for example in Ref. [21].

Another major problem is routing of feedlines (power, propellant, cooling water) from the laboratory system onto the thruster platform. Moving, bending, and pulling of cables and other lines often introduces unknown forces that cannot be attributed to the thruster itself and may generate a bias or significantly influence the accuracy of thrust measurement. Furthermore, the electric and magnetic fields as wells as other oscillatory forces (such as vibrations from cooling liquids) from the electric thruster itself might be

Table 1 Characteristics of basic design concept of thrust balances as shown in Fig. 2

Design type	Advantages	Disadvantages	Fig. 2
vertical weigh cell	• commercial systems are available • simple design	• cell has to carry all weight of thruster assembly • thrust has to be measured against thruster weight	(a)
single arm pendulum	• simple design • high sensitivity	• thruster weight impacts measurement • thrust vector changes in operation w/o displacement compensation • pendulum length is crucial • oscillations may appear	(b)
torsional pendulum	• very sensitive • low forces measurable • thruster weight has theoretically no impact on measurement	• needs to be well balanced • position of thruster must be accurately known • thrust vector changes in operation w/o displacement compensation	(c)
inverted pendulum	• simple design • thruster weight has theoretically no impact on measurement	• active control required • position of thruster must be accurately known	(d)
inverted double pendulum	• thruster weight has theoretically no impact on measurement • high sensitivity • thruster platform stays horizontal • free positioning of thruster	• active control required • complex mechanical design	(e)
counterbalanced inverted pendulum	• thruster platform stays horizontal • free positioning of thruster • by trimming the weight, this system can be very sensitive • thruster weight has theoretically no impact on measurement • inherently stable with counterweights • sensitivity can be tuned	• may need active control • high sensitivity • very complex, many pivoting points	(f)

measured and need to be compensated for, but these effects will not be discussed further within this paper.

Thrust balances at STG-ET

Thrust balances for EP vacuum test facilities are very specialized devices and cannot be purchased off the shelf. Therefore, thrust measurement is performed with unique instruments developed on their own by each test facility. Since 2013 DLR uses a thrust balance built in a cooperation task with the company AST (Advanced Space Technologies, Bremen, Germany). AST has background in EP technology, and the balance development was based on earlier work [7]. This device has prototype status and was especially designed for the application at DLR's EP facility. It is built based on the design of a counterbalanced inverted double pendulum structure.

Table 2 lists the specifications that were given by the manufacturer. In order to reach a maximum in accuracy of thrust measurement, a fine-tuning of the control loop settings to the respective load conditions is required. As a drawback the whole system is very critical with respect to different load conditions. Untuned operation could lead to oscillations or

Table 2 Thrust balance design specifications, as given by manufacturer AST

Parameter	Specification
Maximum thruster mass	40 kg
Thrust range	0–250 mN
Accuracy	2.5 mN
Repeatability	0.5 mN
Resolution	<0.25 mN
Response time (0–90%)	5 s
Settling time	10 s
Drift	< 0.5% of full range per hour
Temperature drift	< 0.1% per deg., measured at thruster platform
Burn-in time	1 hour
Mass	130 kg
Size	height: 697 mm, width: 570 mm, depth: 592 mm
Other features	– calibration with voice coil – calibration with weight – calibration in vacuum – option for 1N full range upgrade

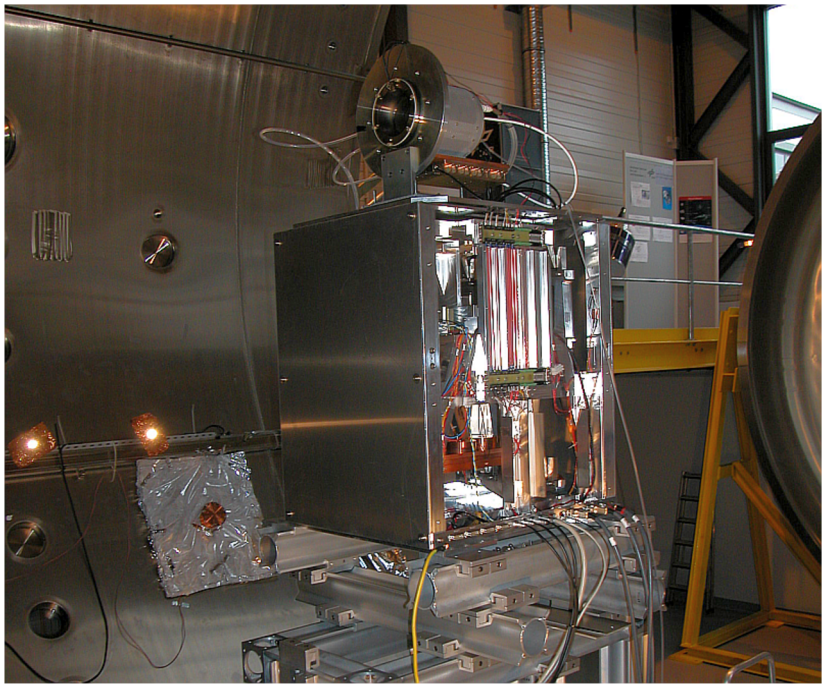

Figure 3 AST thrust balance in the STG-ET with a small radiofrequency ion thruster mounted on it, see [4]

unsteady offset values. Another issue of this special balance is that we observed a long-term drift which is above the specified value.

The thruster plus additional equipment weight has to be compensated by a counter-weight mass on the lower platform in order not to have an unstable setup with a top platform falling into travel limits.

Figure 3 displays the AST thrust balance installed in the STG-ET with a small RIT10 radiofrequency ion thruster mounted on it [4]. This thruster produces a thrust of 1–2 mN, and this is the very low end of the thrust balance measurement range.

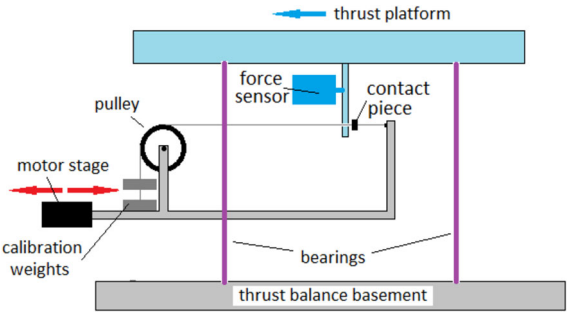

Figure 4 Schematic of the AST thrust stand calibration principle. A motorized motion stage moves to the left, the wire contact piece touches the thrust platform, which then lifts weights. This pulls the thrust platform via a wire and a pulley that transforms the vertical force into a horizontal pull

The AST balance was furthermore used in test campaigns for a RIT22 radiofrequency ion thruster (Ariane Group) and for a Hall effect PPS thruster (Safran).

Calibration system for AST balance

A diagnostics instrument like a thrust balance needs a calibration, and preferably a traceability back to a standard. The AST balance offers two different systems [7]. One is the use of a calibrated voice coil giving a force on the balance, and the second using a weight on a string system. Hereinafter, the weight system is discussed solely.

Figure 4 shows a simplified sketch of the calibration system. The calibration jig contains a pulley and the wire with attached weights. A contact plate is attached to the wire, and in normal operation the wire runs free through a hole in the thrust platform angle bracket. The calibration jig can be moved to the left (in the figure) by a motor stage. As soon as the contact piece touches the bracket the tension in the wire lifts a weight. This leads to a force applied to the thrust platform. Further jig movement will lift a second weight and so on.

A critical point here is friction of the wire on the pulley surface and the stick-slip behavior of the pulley bearings. The calibration procedure compensates this by moving forth and back and taking averages. Due to the small forces involved it may happen that the wire slips over the pulley instead of rotating it. Additionally, the calibration weights might start swinging on the wire, introducing an oscillating force onto the thrust balance.

Figure 5 shows a typical weight calibration plot of the AST thrust balance. The internal weights produce forces of 93.9 mN, 196.9 mN, and 301.9 mN. The calibration process goes up these three steps and down again, producing 5 plateaus. For avoiding as much as possible any backlash or stick-slip errors four forth and back moves are carried out at each calibration point. From Fig. 5 one can see that backlash and stick-slip produce errors of more than tens of mN. The manufacturer stated that averaging the forth and back values at each plateau leads to a correct value. This is to be compared to the nominal forces produced by the weights. With this the calibration can be traced back to the weights, and gives the calibration factor.

The AST thrust balance was used in the STG-ET in several test campaigns using Hall effect or radio frequency ion thrusters.

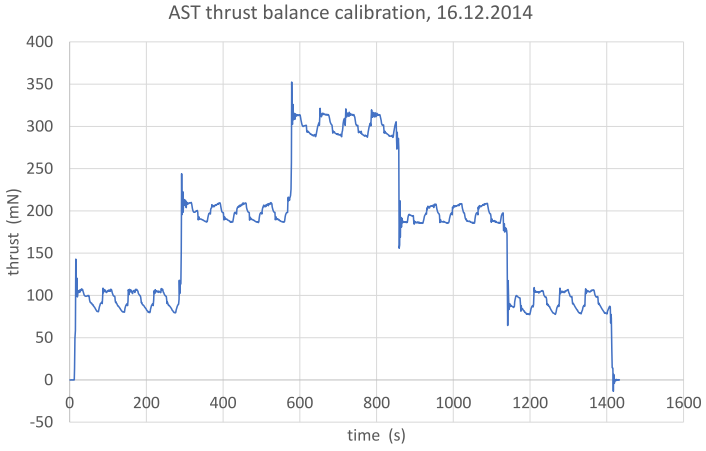

Figure 5 Calibration procedure of the AST thrust balance. Three weight are used, increasing and decreasing the force, and performing four forth and back moves at each calibration point

New thrust balance DEPB

After analyzing the above mentioned test campaigns with the AST thrust balance a few issues appeared, and this triggered the development of the DEPB (**D**LR **E**lectric **P**ropulsion Thrust **B**alance) thrust balance. The ideas behind development of this new system can be listed as:

- to overcome the drawbacks of the AST device: its large size and heavy weight inhibits testing and upgrading the balance in one of DLR's smaller vacuum chambers
- source code not available to DLR: the code cannot be modified or upgraded by DLR
- thermal drift: the observed drift must be lower for long term measurements
- issues with regulation loop: sporadic oscillations appear and the feedback loop optimization is tricky

The new system should fulfil the following specifications:

- device should fit in a small facility with 1 m diameter
- maximum load capacity: 50 kg
- maximum thrust: 500 mN
- full control over calibration procedures
- software code written inhouse by DLR

Thermal drift may be caused by a differential expansion of the bearings and crossmembers of the pendulum design (see Fig. 2(f). Employing design (e) of Fig. 2, merging crossmembers and bearings into one piece, and using a low expansion material (quartz) for these was the adopted option. The thermal expansion coefficient of quartz of $5.1{\cdot}10^{-7}$ K^{-1} up to 100°C. This is more than one order of magnitude lower compared to aluminum which is extensively used in the AST balance. The assembly sketch of the main components of the DEPB device can be seen in Fig. 6. In the figure caption the components are names. The thruster plate is held by the quartz rods—four oriented vertically and four crossed for inhibiting sidewise movements. Technical details about the special features can be found in [22]. Figure 7 shows the open DEPB balance with its quartz rods as flex bearings, and an additionally mounted eddy current brake for oscillation reduction.

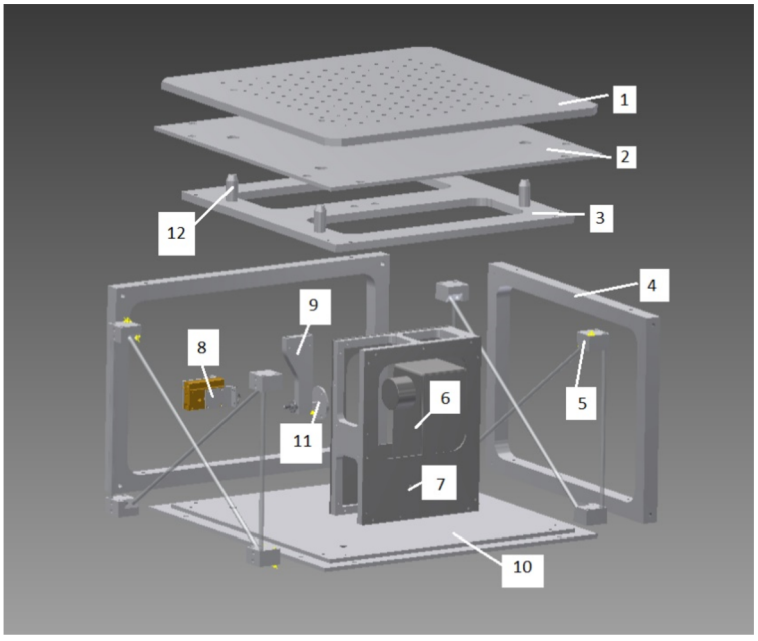

Figure 6 Assembly sketch of the main components of the DEPB device. The eddy current brake not shown here. Parts: 1 thruster platform; 2 housing top plate; 3 upper moving platform; 4 housing frame; 5 flexible bearing rod assembly; 6 weigh cell; 7 weigh cell supporting frame; 8 calibration stage assembly; 9 Force transmission piece with screw; 10 base plate; 11 contact piece; 12 connection stud to thruster platform

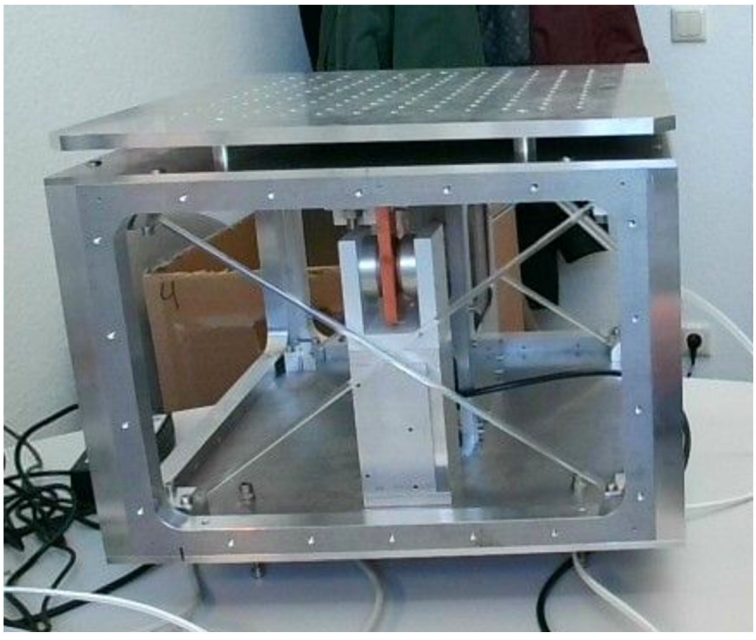

Figure 7 Open DEPB thrust stand. One can see some of the quartz rods holding the top thrust platform. Here, the eddy current brake is mounted: copper plate between two magnets

Weigh cell sensor

The DEPB thrust stand uses a commercial weigh cell (load cell) from Sartorius®, a worldwide known company in the weighing, filtering and pharmaceutical market. The sensor has the reference WZA224, a full range of 220 g and a resolution of 0.1 mg. Its weight is about 2 kg, and it comes with an external control unit and an optional display unit. The communication with a computer is done via a RS232 interface. For simplicity this unit is short-named WZA in the following text. Its measurement principle is based on an actively compensated mechanism with an optical position sensor. The whole unit is well enclosed for different commercial applications. With this sensor we can rely on an often-used product with the profound background knowledge of a well-known company. The drawback is that this WZA unit is neither qualified for vacuum nor for a measurement of horizontal forces. Therefore, extensive qualification tests had to be performed before being able to use the WZA for our purpose. The first question was if the sensor would be able to function in vacuum, e.g. can the internal components withstand vacuum, and is this also valid for the spirit level mounted on the outside. The second question was if the WZA can operate in a position rotated by 90° degrees and measure a horizontal force. This is very different compared to a vertical weighing task, like in the arrangement it was designed for.

After completion of our qualification tests for the weigh cell these questions could be answered positively, although the force range in the vertical arrangement is largely reduced compared to the original orientation. This may be attributed to the internal complex mechanical design, a Sartorius® intellectual property design. We have a maximum measurable force of about 0.8N instead of 2N. But in conclusion, the WZA sensor can be used in the envisaged thrust balance setup.

DEPB calibration

The WZA cell in its tilted position in the DEPB device cannot directly be used as a calibrated force sensor, but only as a sensor giving a force-dependent signal. As the sensor is used in a tilted orientation its internal force calibration is not valid anymore. Furthermore, the sensor is mounted in a system of mechanical components that introduce additional back-pushing forces. This makes a calibration of the new system mandatory. For this task we have different options. The wire/weight/pulley method was discarded here due to high complexity and several issues, such as a very delicate mechanical construction, the slipping of the wire on the bearing and the introduced inaccuracy. A much simpler system was developed and tested separately and, after confirmation of its viability, implemented in DEPB. Figure 8 shows the principle. A spring on a linear motorized stage can produce a horizontal force on measurement device. Figure 9 sketches its implementation in the thrust balance. The horizontal spring force is directly applied to the thrust platform and acts like a thruster. The thrust platform propagates the force onto the WZA sensor, and the latter gives an arbitrary signal. A comparison of the WZA signal with the known force of the spring stage leads to the calibration factor.

Spring stage for calibration

In Fig. 8 a basic coil spring was shown, but such a design may fulfil Hooke's spring law but could bend to one side if compressed. In our application the goal is not to tune the spring for getting Hooke's law but to have a reproducible constant calibration behavior.

Several spring layouts were tested, including the standard cylindrical coil. The final shape is not a cylindrical wound wire but a straight spring steel wire with a 90° bent at

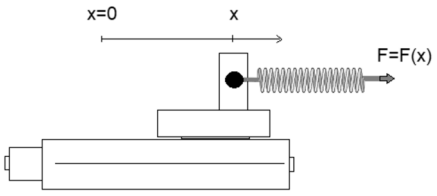

Figure 8 Principle of the DEPB calibration. A calibration spring on its motorized motion stage produces a force F depending on the stage travel x, after contacting

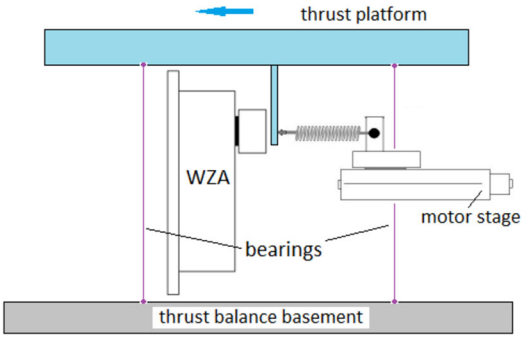

Figure 9 Calibration setup for the DEPB balance design. A motorized stage pushes the calibration spring against the thrust platform. The WZA sensor is show in its arrangement for horizontal force measurement

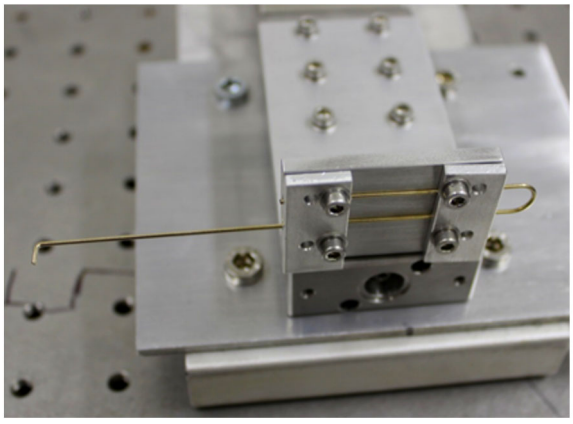

Figure 10 The spring element of the DEPB balance is a single bent wire. The contact point is the bent end on the left, which has a smooth rounded tip

the contact point. It turned out that this shape makes lateral bends much less likely. Figure 10 shows the bent spring wire on the motorized stage. The contact point to the thruster platform is the bent end on the left (see figure), which has a smooth rounded tip that does not punch into the contact surface.

The actuator for the spring stage is a Newport® motorized stage, and its specifications are listed in Table 3.

The spring stage must be calibrated as a system in order to have a function giving force versus stage travel F(x). This calibration is performed in an arrangement shown in Fig. 11. The motorized stage with the spring is mounted above a force measurement device. For convenience we use a second Sartorius® weigh cell, but this time in its nominal orienta-

Table 3 Specifications of Newport® Motion Stage TRA6PPV6 (from data sheet)

Parameter	Value
Travel Range	25 mm
Maximum Speed	1.25 mm/s
Minimum Incremental Motion	100 nm
Accuracy, Typical	$\pm 1.0\ \mu$m
Accuracy, Guaranteed	$\pm 3.0\ \mu$m
Uni-directional Repeatability, Typical	$\pm 0.08\ \mu$m
Uni-directional Repeatability, Guaranteed	$\pm 0.15\ \mu$m
Bi-directional Repeatability, Typical	$\pm 0.2\ \mu$m
Bi-directional Repeatability, Guaranteed	$\pm 1.0\ \mu$m
Drive Type	DC Motor
Origin Repeatability	$\pm 2.5\ \mu$m
Vacuum Compatibility	10^{-6} hPa
Weight	0.73 kg

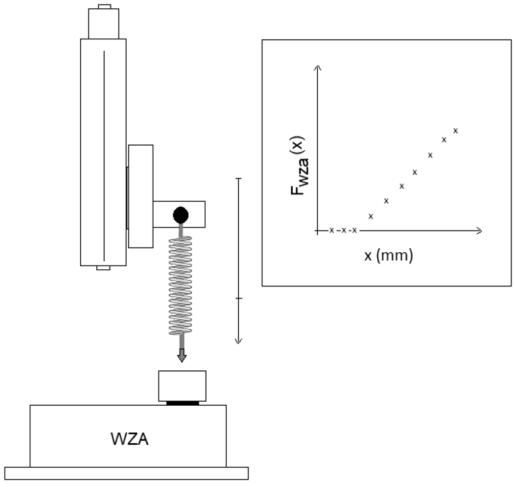

Figure 11 Setup for calibration the spring. A WZA load cell is used in its ordinary position (horizontal) and the motion stage pushed the spring against it. For simplicity sake we still show a wound wire spring. After getting contact the force increases with stage travel (see right inset graph)

tion, and this results in a valid calibration of measured forces. The motion stage moves the spring vertically downwards touching the WZA and producing a force. This is schematically shown in the inset graph on the right.

Figure 12 plots the recorded force data (crosses) versus the stage travel for an exemplary run. The travel range starts at 0 mm and goes up to 9.5 mm, which gives 500 mN of force. This is the maximum force that we need, according to the initially set specifications. The spring may work a little further, but the reversible behavior deteriorates beyond about 10 mm.

Trying to fit the data shows that a linear approach can well be used from about 3 to 6 mm travel. Then we observe a reproducible kink with an increase in slope. This behavior is not what is expected by Hooke's law, but here we may not expect an ideal behavior as mentioned above.

After this kink, a second more linear slope appears in the travel range 6 to about 9.5 mm. The kink may come from the geometry of the spring element in conjunction with its mounting. It may have been possible to connect two linear fits, but we would have to deal

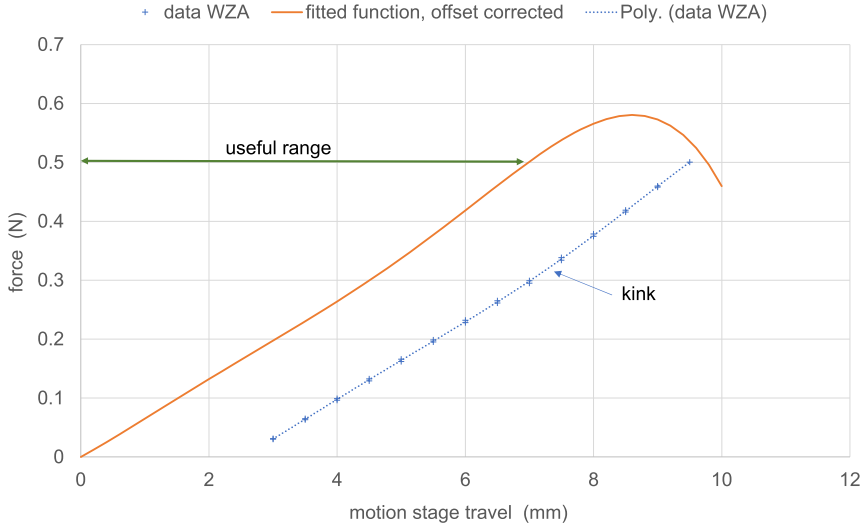

Figure 12 Spring force versus motion stage travel data. Shown are data (crosses), a polynomial fit of order 5 through the data points, and this fit shifted to left passing the origin in its quasi-linear part (solid line)

with the not well-defined position of the kink. Therefore, a polynomial fit was tried as a better and more soft approach. For an acceptable result we have to choose a fifth order polynomial of form:

$$F_{\text{spring}}(x) = C_{s5} \cdot x^5 + C_{s4} \cdot x^4 + C_{s3} \cdot x^3 + C_{s2} \cdot x^2 + C_{s1} \cdot x + C_{s0}\ [N]. \tag{1}$$

The need for 5th order comes from aiming at a correlation coefficient below 0.9999 for the fit to data. Data and fit (dotted line across the data) are shown in Fig. 12. The next step is to shift and normalize the fit so that $\tilde{F}_{\text{spring}}(x = 0) = 0$, which results in finding the zero points. Polynomials might have more than one zero point, but we need the zero point closest to the data left side (the quasi-linear part). The zero point then identifies the point of contact of the spring to the WZA. With that we have the new function:

$$\begin{aligned}\tilde{F}_{\text{spring}}(x) = {} & C_{s5} \cdot (x + x_0)^5 + C_{s4} \cdot (x + x_0)^4 + C_{s3} \cdot (x + x_0)^3 + C_{s2} \cdot (x + x_0)^2 \\ & + C_{s1} \cdot (x + x_0) + C_{s0}.\end{aligned} \tag{2}$$

For the data set shown in Fig. 12 the numerical values for Eq. (2) are:

$$C_{s5} = -0.00004316 \left[\frac{N}{mm^5}\right],$$

$$C_{s4} = +0.00127109 \left[\frac{N}{mm^4}\right],$$

$$C_{s3} = -0.01401273 \left[\frac{N}{mm^3}\right],$$

$$C_{s2} = +0.07285354 \left[\frac{N}{mm^2}\right],$$

$$C_{s1} = +0.11305771 \left[\frac{N}{mm}\right],$$

$C_{s0} = 0\ [N]$.

The fit has been forced to pass zero, and this is shown by elimination of $C_{s0} = 0$. This constraint would not have been necessary but allowing a constant value only marginally improves the accuracy.

With this fit we are able to calculate the offset of x needed for Eq. (2):

$$x_0 = 2.51378\ [\text{mm}]. \tag{3}$$

Pasting the above coefficients into Eq. (2) gives the spring force for x-values starting at zero, i.e. the point of contact. This is necessary because the motion stage travel up to a contact point is different in the spring calibration setup compared to its mounting position in the thrust balance.

The final calibration function for the mentioned spring calibration data is:

$$\begin{aligned} F(x) = &-0.00004316 \cdot (x + x_0)^5 + 0.00127109 \cdot (x + x_0)^4 - 0.01401273 \cdot (x + x_0)^3 \\ &+ 0.07285354 \cdot (x + x_0)^2 - 0.11305771 \cdot (x + x_0). \end{aligned} \tag{4}$$

One comment must be made here. One may be tempted to use the fitted function for extrapolating to larger x values. Using Eq. (4) and extending the calibration to values outside the data pool (solid line in Fig. 12) clearly shows that the polynomial will produce wrong results. Such a risk would be lower if we would have used a linear fit in the first place. But in our case the travel range must be confined to 7 mm after point of contact for avoiding the issue of wrong extrapolation. Travel values below zero are not possible due to the travel limit of the motorized stage.

In summary, with the motion stage mounted in the DEPB we are able to apply calibrated forces from 0 up to 500 mN to the thruster platform.

Software

The DEPB user interface is designed around the commercial components like the weigh cell and the motorized motion stage. It allows to perform the above-mentioned calibration which generates a specific file with the actual calibration data. The WZA features a tare command which is needed for its commercial weight balance applications. This option is not used here but the offset is corrected in the DEPB controller software in conjunction with the calibration function.

Long term data recording can be done within a user-defined interval. A second option permits a recording with maximum data acquisition rate, which is around 20 Hz depending on filter settings and interface communication speed. In this mode the software only offers a limited maximum number of data for preventing communication data storage overflow. When using fast data acquisition, the WZA internal setting must be selected for a very low noise environment, which means using the smallest averaging window. The feature of high-speed data acquisition should only be used with care and during fast response tests.

Cooled enclosure

For keeping the DEPB balance at a constant temperature the balance frame was equipped with cooled sidewalls. This cooling system is different from the approach used for the

Figure 13 DEPB device in a cleanroom tent with closed sidewalls and watercooled plates attached to the sides

Table 4 Impact of cooled DEPB sidewalls

	Setup details		
	No walls	With walls, cooling OFF	With walls, cooling ON
measurement date	21.07.2018	04.08.2018	11.08.2018
thrust standard deviation	$1.05 \cdot 10^{-3}$ mN	$8.01 \cdot 10^{-4}$ mN	$6.43 \cdot 10^{-4}$ mN

AST balance, which is controlled heated to a temperature above ambient. The balance with its coolers is shown in Fig. 13 during a test in a cleanroom for evaluating the thermal stability. The idea was to run the system over a few days and observe the balance behavior responding to the daily room temperature variation. Table 4 shows the results of balance operation without sidewalls, with sidewalls but no cooling water flow, and finally with a cooling water flow of 24°C. The evaluation parameter is the standard deviation of the recorded thrust measurement (in mN). Fitting sidewalls improve the stability of the measurement over time by an order of magnitude. The cooling water flow adds a further improvement of about 20%, and this is valid for an environment without additional heat sources.

First results with the DEPB system

At the moment, the DEPB device is in a development status and did not yet run in conjunction with a real EP thruster. A very critical point is the routing of cables and feed lines from the fixed chamber environment onto the thruster platform. A wrong placement or tensioning of these leads to bias or other disturbing effects. Therefore, a first qualification was be done without a thruster. An electromagnetic push mechanism for thruster simulation was set up. Figure 14 shows this mechanism, which is made of a relay coil with an attached pushrod. The coil can be actuated by a DC current, and the pushrod simulates a thrust force. By tuning the DC current a force close to full scale can be obtained, and a value of 0.87N was selected. With this simple device basic response tests are feasible.

In Fig. 15 we have the data record of a step function of 0.87N lasting for about 6 s, produced by the coil pushrod device. It is interesting to see the rise time of the system for an estimation of the measurable pulses. In Fig. 16 the rise time is determined by the time needed to step from 10% signal up to 90% signal. The result is a time of 0.24 s.

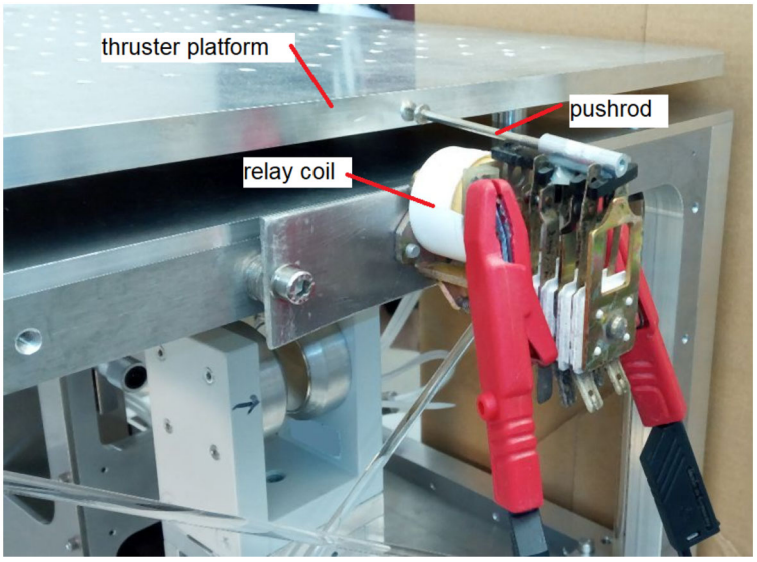

Figure 14 Force actuator made of a relay with a pushrod

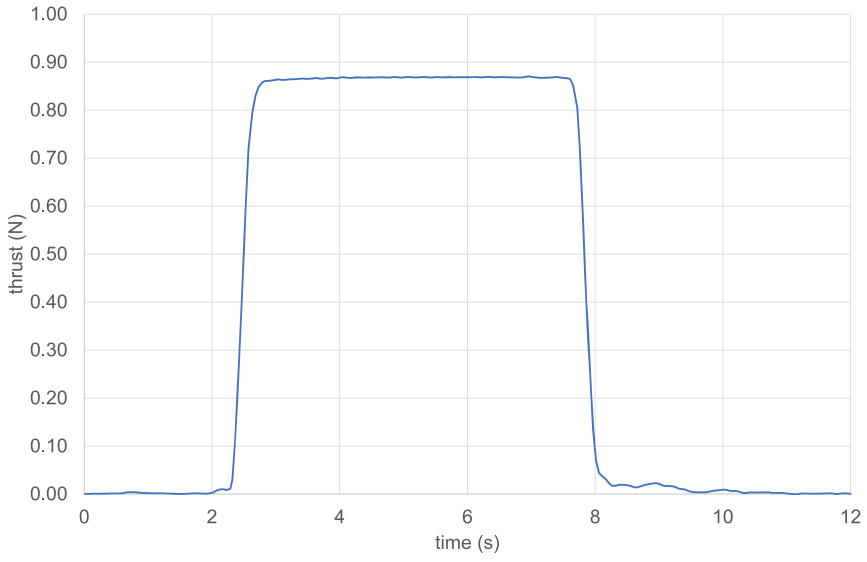

Figure 15 Recording of a load step generated by the force actuator

A sequence of fast pulses was recorded in the fast data acquisition mode, and this is shown in Fig. 17. The balance is able to measure pulses down to a repetition rate of 1 Hz. Such repetition rates may be useful for testing thrusters in a pulsed firing mode. Pulses occurring at a higher rate can still be resolved, but absolute value is not correct which is explained by the rise time of 0.24 s.

Summary and conclusions

For the future challenges in electric propulsion, especially low-power, low-thrust thrusters, which are feasible for the growing market of cubesats and small satellites, new and more

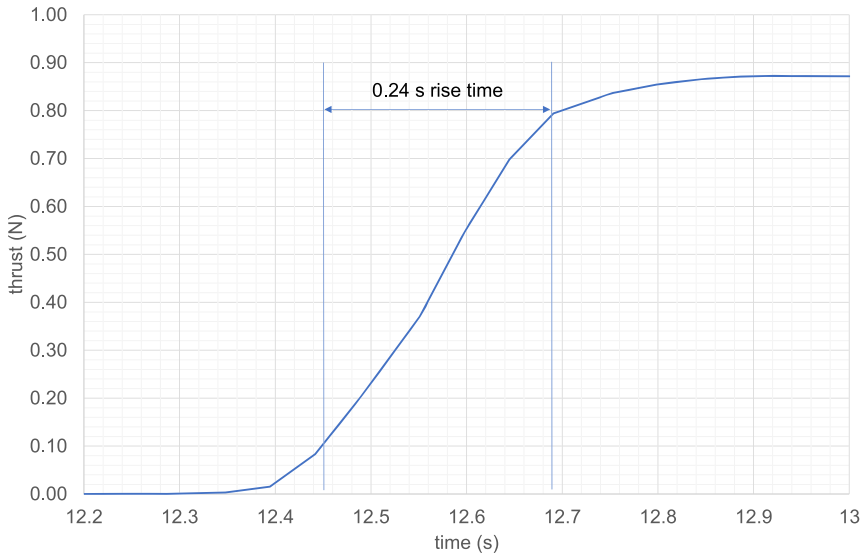

Figure 16 Determination of the rise time of the balance. The 10% to 90% rise time of the balance is 0.24 s

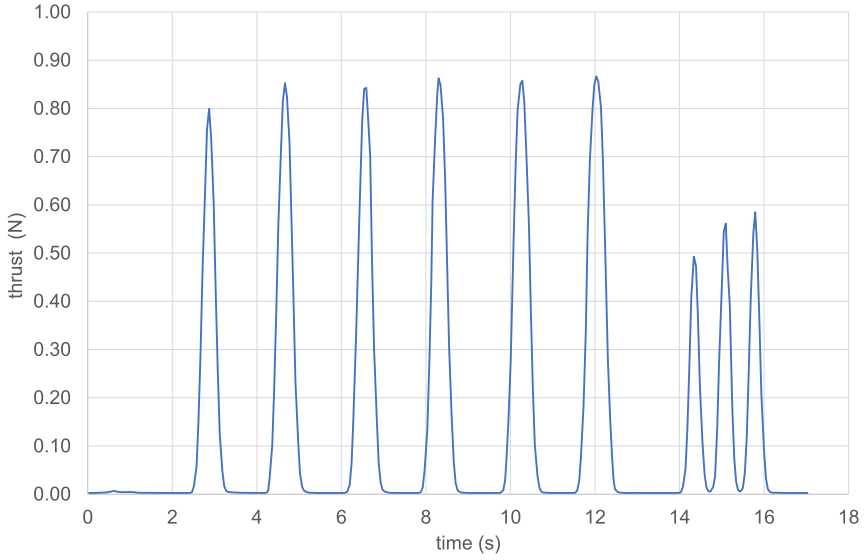

Figure 17 Recording in fast mode with maximum acquisition frequency of 20 Hz. The spikes correspond to load pulses generated by the force actuator

accurate methods of thrust measurement for small forces are necessary [23]. These thrust balances need to be thermally stable for extended periods of time to ensure the qualification. Since these smaller thrusters often also have less weight, it is often more convenient to use smaller thrust balances.

For thrust measurement at the STG-ET facility the AST balance has been used, which has been described here. The new DEPB thrust balance currently under development at DLR Göttingen has been presented and the design considerations were shown which lead to the optimizations in comparison to the AST thrust balance. The thrust platform is con-

nected to the base plate by fixed quartz rods due to their very small thermal expansion to minimize the influence of thermal gradients which often occur during long-term testing. The force sensor is a commercially available load cell by Sartorius®, and the calibration is done by a simple calibrated spring system based on a bent wire on a motorized linear stage. The overall design is more compact and fits into a 1 m^3 vacuum chamber.

Preliminary tests with this new thrust balance showed promising results concerning accuracy and ease of calibration, mainly due to the improvement of the sensor and calibration mechanism in contrast to the larger thrust balance.

In the near future we will collect results from more tests with a real EP thruster to demonstrate the full functionality and thermal stability of the thrust stand under vacuum conditions. Additionally, it will be of high interest to study the behavior of a thrust balance under the influence of vibrations and strong magnetic fields.

Acknowledgements
The authors would like to thank Patrick Dahm for design and mechanical construction of the DEPB device, and its first tests within a bachelor thesis. Elena Zorzoli Rossi added thermal simulations and a complete cooling plate set in order to keep the thrust balance thermally stable. This was done within her master thesis. Further thanks are due to Michael Neumann for performing tests of the Sartorius® WZA sensor under vacuum, and investigating the degree of movement of the weigh cell head under different loads, all this within an internship work.

Funding
Open Access funding enabled and organized by Projekt DEAL.

Abbreviations
DEPB, DLR Electric Propulsion Thrust Balance; EP, Electric Propulsion; RIT, Radio Frequency Ion Thruster; STG-ET, Simulationsanlage Treibstrahlen Göttingen—Elektrische Triebwerke.

Availability of data and materials
Not applicable.

Declarations

Competing interests
The authors declare that they have no competing interests.

Authors' contributions
AN and JSi are involved in EP thrust balance design since many years. AN initiated the DEPB development and wrote the draft manuscript. JSi and JSc added sections and assisted in proof reading. All authors read and approved the final manuscript.

Publisher's Note

Received: 18 August 2021 Accepted: 18 October 2021 Published online: 23 November 2021

References

1. Levchenko I, Xu S, Mazouffre S, Lev D, Pedrini D, Goebel D, Garrigues L, Taccogna F, Bazaka K. Perspectives, frontiers, and new horizons for plasma-based space electric propulsion. Phys Plasmas. 2020;27:020601. https://doi.org/10.1063/1.5109141.
2. Kreiner K. The future of satellite propulsion. In: EUCASS 2013, 5th European Conference for Aeronautics and Space Sciences. Presentation, Munich, Germany, 1–5 July 2013. https://www.eucass.eu/2013/pdf/EUCASS2013-Boeing-Kreiner-Future_of_Satellite_Propulsion.pdf. Accessed 5 July 2021
3. Neumann A. STG-ET: DLR electric propulsion test facility. J Large-Scale Res Facil. 2018;4:A134. https://doi.org/10.17815/jlsrf-3-156-1.
4. Neumann A. Update on diagnostics for DLR's electric propulsion test facility. Proc Eng. 2017;185:47–52. https://doi.org/10.1016/j.proeng.2017.03.289.
5. Polk JE, Pancotti A, Haag T, King S, Walker M, Blakely J, Ziemer J. Recommended Practices in Thrust Measurements. In: Proceedings of the 33rd International Electric Propulsion Conference, Washington, DC, October 6–10. Paper No. IEPC-2013-440, 2013
6. Gonzales del Amo J, Saccoccia G, Frigot P-E. ESA Propulsion Lab at ESTEC. In: Proceedings of the 31st International Electric Propulsion Conference, Ann Arbor, Michigan, USA. Paper No. IEPC-2009-236, 2009

7. Neumann A, Sinske J, Harmann H-P. The 250 mN Thrust Balance for the DLR Goettingen EP Test Facility. In: Proceedings of the 33rd International Electric Propulsion Conference, The George Washington University, Washington DC, USA, October 6–10. Paper No. IEPC-2013-211, 2013
8. Packan D, Bonnet J, Rocca S. Thrust Measurements with the ONERA Micronewton Balance. http://electricrocket.org/IEPC/IEPC-2007-118.pdf. Accessed 26 July 2021
9. Kang SJ, Cho HR, Chang Y. Development and testing of a micro-thruster impulse characterization system utilizing pendulum swing time measurements. Sens Actuators A, Phys. 2008;148(2):381–7. https://doi.org/10.1016/j.sna.2008.09.004.
10. Polzin KA, Markusic TE, Stanojev BJ, DeHoyos A, Spaun B. Thrust stand for electric propulsion performance evaluation. Rev Sci Instrum. 2006;77:105108. https://doi.org/10.1063/1.2357315.
11. Yang Y-X, Tu L-C, Yang S-Q, Luo J. A torsion balance for impulse and thrust measurements of micro-Newton thrusters. Rev Sci Instrum. 2012;83:015105. https://doi.org/10.1063/1.3675576.
12. Gamero-Castaño M. A torsional balance for the characterization of microNewton thrusters. Rev Sci Instrum. 2003;74(10):4509–14. https://doi.org/10.1063/1.1611614.
13. Boccaletto L, d'Agostino L. Design and Testing of a Micro-Newton Thrust Stand for FEEP. In: 36th Joint Propulsion Conference, 17–19 July 2000, Huntsville, AL, USA, AIAA-2000-3268, 2000
14. Hathaway G. Sub-micro-Newton resolution thrust balance. Rev Sci Instrum. 2015;86:105116. https://doi.org/10.1063/1.4933382.
15. Soni J, Roy S. Design and characterization of a nano-Newton resolution thrust stand. Rev Sci Instrum. 2013;84:095103. https://doi.org/10.1063/1.4819252.
16. Kokal U. Development of BUSTLab Thrust Stand for mili-Newton Level Thrust Measurements of Electric Propulsion Systems. Master thesis, Boğaziçi University, Turkey; 2019. Accessed 5 July 2021
17. Walker MLR, Xu KG. High-power, null-type, inverted pendulum thrust stand. Rev Sci Instrum. 2009;80:055103. https://doi.org/10.1063/1.3125626.
18. Stephen RJ, Rajanna K, Dhar V, Kalyan Kumar KG, Nagabushanam S. Thin-film strain gauge sensors for ion thrust measurement. IEEE Sens J. 2004;3:373–7. https://doi.org/10.1109/JSEN.2004.827276.
19. Nagao N, Yokota S, Komurasaki K, Arakawa Y. Development of a two-dimensional dual pendulum thrust stand for Hall thrusters. Rev Sci Instrum. 2007;78:115108. https://doi.org/10.1063/1.2815336N.
20. Harmann H-P, Koch N, Kornfeld G. The ULAN Test Station and its Diagnostic Package for Thruster Characterization. In: International Electric Propulsion Conference, IEPC-2007-119, September 17–20, 2007. http://electricrocket.org/IEPC/IEPC-2007-119.pdf. Accessed 5 July 2021
21. Banetta S, Falorni R, Biagioni L. Development of a two-axes thrust stand for electric thrusters. In: A. Wilson, editor. Proc. 4th Int. Spacecraft Propulsion Conference (ESA SP-555), 2–9 June, 2004, Chia Laguna (Cagliari), Sardinia, Italy. Published on CDROM., id.121.1. October 2004. Bibcode: 2004ESASP.555E.121B
22. Neumann A, Dahm P. Patent, Germany, No. DE 10 2017 100 876 B4, 2.7.2019
23. Levchenko I, Bazaka K, Ding Y, Raitses Y, Mazouffre S, Henning T, Klar PJ, Shinohara S, Schein J, Garrigues L, Kim M, Lev D, Taccogna F, Boswell RW, Charles C, Koizumi H, Shen Y, Scharlemann C, Keidar M, Xu S. Space micropropulsion systems for cubesats and small satellites: from proximate targets to furthermost frontiers. Appl Phys Rev. 2018;5:011104. https://doi.org/10.1063/1.5007734.